Neoplasia • Vol. 8, No. 12, December 2006, pp. 1011–1018 1011

www.neoplasia.com

In Vivo Imaging of Molecularly Targeted Phage

Kimberly A. Kelly, Peter Waterman and Ralph Weissleder

Center for Molecular Imaging Research, Massachusetts General Hospital, Harvard Medical School, Boston, MA, USA

Abstract

Rapid identification of *in vivo* affinity ligands would have far-reaching applications for imaging specific molecular targets, *in vivo* systems imaging, and medical use. We have developed a high-throughput method for identifying and optimizing ligands to map and image biologic targets of interest *in vivo*. We directly labeled viable phage clones with far-red fluorochromes and comparatively imaged them *in vivo* by multichannel fluorescence ratio imaging. Using Secreted Protein Acidic and Rich in Cysteine (osteonectin) and vascular cell adhesion molecule-1 as model targets, we show that: 1) fluorescently labeled phage retains target specificity on labeling; 2) *in vivo* distribution can be quantitated (detection thresholds of ~ 300 phage/mm^3 tissue) throughout the entire depth of the tumor using fluorescent tomographic imaging; and 3) fluorescently labeled phage itself can serve as a replenishable molecular imaging agent. The described method should find widespread application in the rapid *in vivo* discovery and validation of affinity ligands and, importantly, in the use of fluorochrome-labeled phage clones as *in vivo* imaging agents.

Neoplasia (2006) **8,** 1011–1018

Keywords: Phage display, screening, drug discovery, molecular imaging, systems biology.

Introduction

Molecularly targeted affinity ligands derived from screens play an important role in our further understanding of human disease [1–4], pharmaceutical discovery and development [5–7], nanotechnology sensing applications [8], systems biology [9], and the design of molecular imaging agents [10–13]. Various types of high-throughput screens, including small molecule screens [14,15], yeast two-hybrid screens [16], bacterial display screens [17], and phage display screens [5,10,18,19], have been developed. The latter offers a number of important advantages, such as rapid and economical biologic expansion (rather than the more time-consuming chemical resynthesis), vast peptide diversity, rapid screening process, and the availability of many types of phage clones and libraries (for a review, see Smith and Petrenko [20] and Willats [21]).

A number of modifications to traditional phage screens have been developed over the last decade. Traditional *in vitro* screens commonly use purified target proteins immobilized on plates [22]. Alternatively, screens have been performed on live cells, with targets expressed in their native environments, which has allowed the development of modified screens that bias toward cell internalized phage [23,24], binding under flow conditions [10] or other biologic processes. One of the most exciting recent developments has been the use of *in vivo* phage display to yield disease-specific or organ-specific phage clones [18,19]. For example, a number of atherosclerosis-targeted phage have recently been developed [25], and endothelial bed–specific clones have been found in both mice and humans [2,26]. However, irrespective of the method employed, it is common for a given screen to yield tens to hundreds of potential phage clones that subsequently require time-consuming and costly validation. In addition, once a clone is validated, developing, validating, and scaling up an imaging agent based on lead peptides can be challenging and costly.

Given the existing bottlenecks in identifying clones with the highest likelihood of *in vivo* success and to determine if we could use phage as a targeted imaging agent, we set out to develop comparative *in vivo* screening tools. We reasoned that such comparative screens could be of value in eliminating *in vitro*–identified clones that would ultimately fail because of unfavorable *in vivo* pharmacokinetics, delivery barriers, opsonization, or insufficiently high target-to-background ratios [27,28]. Specifically, we applied far-red and near-infrared fluorescent labeling and newer *in vivo* fluorescence methods to track phage *in vivo* to intended targets of interest. Using Secreted Protein Acidic and Rich in Cysteine (SPARC) as a model target for invasive cancer [29,30] and vascular cell adhesion molecule-1 (VCAM-1) for inflammatory endothelium [31], we show how novel targeted peptide sequences can be rapidly developed. We furthermore show that individual fluorescently labeled phage clones can be remarkably efficient as *in vivo* imaging agents, akin to peptide-decorated nanoparticles [32].

Address all correspondence to: Ralph Weissleder, MD, PhD, Center for Molecular Imaging Research, Massachusetts General Hospital, Room 5403, Building 149, 13th Street, Charlestown, MA 02129. E-mail: weissleder@helix.mgh.harvard.edu

Received 27 September 2006; Revised 27 September 2006; Accepted 2 October 2006.

DOI 10.1593/neo.06610

Materials and Methods

Materials

N-hydroxysuccinimide esters of Cy3.5 and Cy5.5 were obtained from Amersham (Piscataway, NJ); fluorescein isothiocyanate (FITC) and tetramethyl rhodamine isothiocyanate (TRITC) were from Sigma Aldrich (St. Louis, MO); *N*-hydroxysuccinimide esters of Vivotag-680 (VT680) and Angiosense-750 were from Visen Medical (Woburn, MA); and *N*-hydroxysuccinimide esters of AF750 were from Invitrogen (Eugene, OR). All other chemicals were purchased from Sigma Aldrich or Pierce (Rockford, IL) and used as received.

Phage Libraries

The SPARC-targeted phage used in this study was isolated from the linear 7 mer library (PhD 7), and the VCAM-1–targeted phage was isolated from the disulfide constrained cyclic 7 mer phage display peptide library (PhD C7C; New England Biolaboratories, Cambridge, MA).

Selection of Targeted Phage Clones

To identify SPARC-targeted clones, phages [2×10^{11} plaque-forming units (pfu)] were incubated for 1 hour at 37°C in a well containing purified SPARC protein (Hematologic Technologies, Inc., Essex Junction, VT) that was adsorbed (100 μg/ml) onto MaxiSorp immunoplates (Nalge Nunc, Rochester, NY) and saturated with bovine serum albumin (BSA). Following incubation, unbound phages were removed by 10 washes with Dulbecco's phosphate-buffered saline (DPBS) containing 1% BSA and 0.1% Tween-20. Bound phages were eluted with 100 μl of acidified glycine buffer (0.2 M glycine, pH 2.2) and neutralized with 10 μl of 1 M Tris (pH 9.0) to preserve viability. The eluted phage pool was then amplified, titered, and subjected to three additional rounds of SPARC selection, and individual clones were selected for enzyme-linked immunosorbent assay (ELISA) and sequencing. VCAM-1–targeted phage clones were selected and validated as previously described [10]. A clone expressing the peptide sequence CVHSPNKKC was used for fluorescent labeling.

ELISA Assay

Purified SPARC protein or BSA adsorbed (20 μg/ml) on Nunc MaxiSorp plates (4°C overnight) was incubated at room temperature with phage clones (10^{12} pfu, 1 hour), washed with DPBS containing 1% BSA and 0.1% Tween-20, incubated with biotinylated anti-M13 antibody (Amersham Pharmacia Biotech, Piscataway, NJ) (1:40, 1 hour), detected with streptavidin–horseradish peroxidase (1:500), and developed with tetramethyl benzidine (Pierce), and absorbance was determined at 650 nm (E_{max}; Molecular Devices, Sunnyvale, CA). Specificity was determined by dividing SPARC abs 650 nm by BSA abs 650 nm.

Phage Labeling

Phages were labeled with a number of different fluorochromes. Fluorochromes were all conjugated to the phage using standard NHS or isothiocyanate chemistry. Phages (1×10^{12} pfu) were resuspended in 100 μl of a 0.3-M $NaHCO_3$ (pH 8.6) solution containing 1 mg/ml fluorochrome–hydroxysuccinimide ester (Cy3.5, Cy5.5, VT680, and AF750) or 0.25 mg/ml FITC (TRITC). The phage/fluorochrome reaction was allowed to continue for 1 hour at room temperature in the dark. Subsequent to incubation, the volume of the labeled phage was brought up to 1 ml with DPBS, and the phage was purified by polyethyleneglycol precipitation. Fluorochrome-labeled phage was then resuspended in 200 μl of DPBS and titered to determine plaque-forming units, and the concentration of fluorochrome was determined spectrophotometrically (Varian Cary II; Varian, Palo Alto, CA).

In Vitro *Characterization of Labeled Phage*

1. Fluorochromes/phage: the number of fluorochromes bound per phage was determined by comparing the concentration of fluorochrome in the sample as determined spectrophotometrically in the phage titer.
2. Fluorescence as a function of labeling: the fluorescence of phage with increasing dye loading was quantified by fluorescence spectroscopy (Fluorolog2; Jobin Yvon Horiba, Edison, NJ). For *in vivo* experiments, we chose phage with a dye loading of 800 fluorochromes/phage due to optimized signal *versus* quenching.
3. Viability of fluorochrome-labeled phage: phages labeled with increasing amounts of fluorochrome were titered using New England Biolabs (NEB) protocols to determine their ability to transfect and amplify in *Escherichia coli*.

Mouse Models

Nude mice were injected subcutaneously with 2.5×10^6 Lewis lung carcinoma (LLC) cells in both flanks. Tumors were allowed to grow until they had reached a diameter of 7 to 10 mm before the animals were used for experimentation. To induce microvascular VCAM-1 upregulation, C57Bl/6 mice ($n = 10$) were injected subcutaneously in the right ear with 5 ng/50 μl mTNFα in normal saline. After 24 hours, animals were anesthetized with inhaled isoflurane and injected intravenously (through the tail vein) with VT680-labeled VCAM-1–targeted phage.

In Vivo *Imaging of LLC Tumor-Bearing Mice*

For the time course experiment (Figure 3*A*), mice ($n = 10$) were coinjected with VT680-labeled SPARC-targeted phage and AF750-labeled wild-type (no insert) phage at equal fluorochrome concentrations and then imaged 2, 4, 6, and 24 hours postinjection. For clone comparison studies (Figure 5*A*), mice ($n = 5$ per clone) were also coinjected with VT680-labeled SPARC-targeted phage and AF750-labeled wild-type (no insert) phage through the tail vein then imaged 4 hours postinjection. In Figures 3*C* and 4, mice ($n = 10$) were injected with either VT680-labeled SPARC-targeted phage or VT680-labeled wild-type phage (no insert) then imaged 4 hours postinjection with surface reflectance imaging and fluorescent molecular tomography (FMT). Mice were anesthetized by inhalation anesthesia (2% isoflurane, 1 l/min O_2).

FMT experiments were performed at two wavelengths (at 680/700 nm to detect SPARC-targeted phage and at 750/780 nm to detect wild-type phage excitation/emission) in anesthetized mice [33]. Briefly, mice were positioned and surrounded by matching fluid to simulate tissue properties according to the manufacturer's instructions (Visen Medical). Image data sets were reconstructed using a normalized Born forward model adapted to small mouse models [33]. Image acquisition time per animal was 2 minutes, and reconstruction time was 1 to 2 minutes. Images were displayed as raw data sets (excitation, emission, and masks) and as reconstructed 3D data sets in axial, sagittal, and coronal planes. Fluorochrome concentration in the target was automatically calculated from reconstructed images and expressed as picomoles of fluorochrome per defined target volume. In addition to the 3D FMT described above, we also performed rapid fluorescence screening using reflectance detection only (Figure 3*C*). This method allowed for a throughput of > 20 mice/hour.

Intravital Laser Scanning Microscopy

Multichannel fluorescence imaging was performed with a prototypical laser scanning fluorescence microscope (Olympus Corporation, Tokyo, Japan) specifically developed for intravital imaging of mouse organs [34]. Three laser lines at 488, 633, and 748 nm were used. Image acquisition was 1 second. The FluoView 300 software program (Olympus Corporation) was used to control the microscope and to collect images of 512 × 512 pixels with a pixel size of about 5.4 μm/pixel and a total image size of about 2.8 × 2.8 mm. Images were stored as multilayer 16-bit tagged image file format files. Images in the 680-nm channel (660- to 730-nm bandpass filter) and in the 750-nm channel (770-nm longpass filter) were collected concomitantly using custom-made filters and dichroic mirrors (Olympus Corporation). A dry objective (×4 UplanApo NA 0.16; Olympus Corporation) with a field of view of 3.25 mm and a theoretical lateral resolution of about 2.6 μm at 680 nm were used. Wide spectral response photomultiplier tubes (model R928P; Hamamatsu, Bridgewater, NJ) were used as detectors for both visible light and near-infrared signals. After initial images had been obtained, a near-infrared vascular imaging agent (Angiosense-750) was administered to define microvascularity [35].

Histology

Epifluorescence microscopic images were obtained with an upright fluorescence microscope (Eclipse 80i; Nikon Instruments, Melville, NY) with a cooled charge-coupled device camera (Cascade 512B; Photometrics, Tucson, AZ). After imaging by intravital confocal microscopy, immunohistochemical analysis of mouse ears was performed. Frozen sections were stained for the presence of CD31, VCAM-1, or M13. Digital images were taken using a Nikon Eclipse E400 upright microscope (×40 objective; Nikon Instruments) equipped with an Insight color camera (Diagnostics Instruments, Sterling Heights, MI).

Results

A number of commercially available fluorochromes were initially used to test the labeling efficiency of M13 phage coat proteins through hydroxysuccinimide or isothiocyanate chemistry, yielding fluorescent phage clones. Figure 1 summarizes the optical properties of differently-labeled M13 phage. Assuming a 6-mm depth in tissues, near-infrared–labeled phages would be detectable roughly 10^2-fold more efficiently compared to labeled phages in the visible spectrum. Therefore, we particularly focused on far-red and near-infrared fluorochromes as light penetration *in vivo* is more efficient at these wavelengths [36]. To better understand the effect of labeling efficiency on phage affinity, fluorescence, and viability, we subsequently performed more in-depth experiments on a phage labeled with a fluorochrome with an excitation wavelength of 680 nm (VT680).

Figure 2 summarizes the effect of the incremental modification of phage coat proteins on the fluorescence, affinity, and viability of isolated phage clones. As a model system, we used one clone (clone 23) isolated from a selection against

A.

Fluoro-chrome	Fl/phage	Ex/Em	Relative SNR at 6 mm depth*
FITC	720	480/510	1.1
TRITC	745	541/572	0.5
Cy3.5	848	541/596	5
Cy5.5	773	680/700	81
VT680	720	680/700	81
AF750	717	750/770	100

* calculated based on mouse tissue absorption

B.

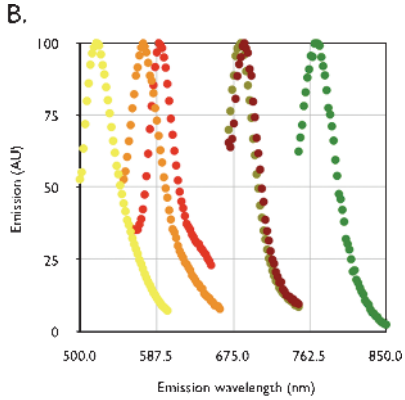

Figure 1. *Phage labeling. (A) Fluorochromes used for phage labeling. Listed are the mean numbers of fluorochromes from a single comparative experiment. The relative fluorescence signal at a 6-mm tissue depth of different fluorochrome-labeled phages was calculated from known spectral tissue absorption. Note the much higher fluorescence of 680- to 750-nm fluorochrome-labeled phages in tissues. (B) Emission spectra of fluorescently labeled phages (excitation and color of data points as listed in A).*

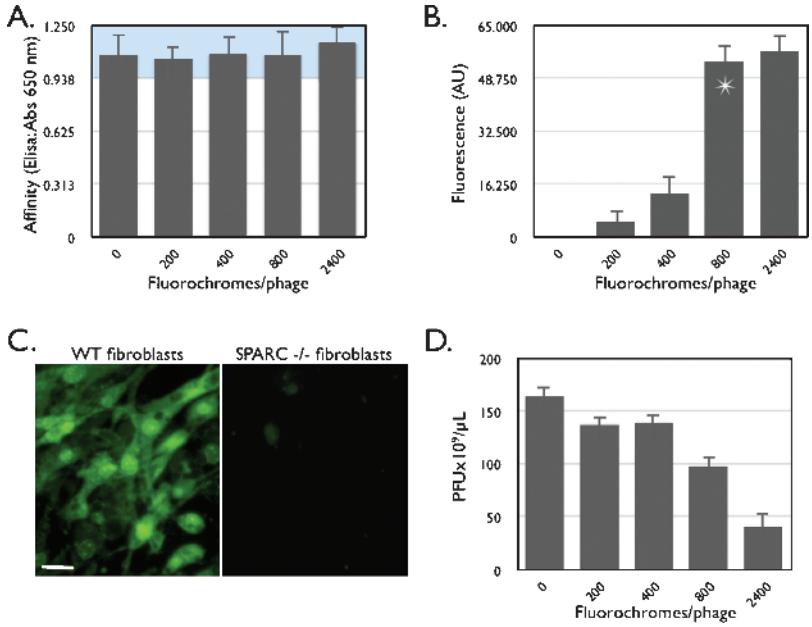

Figure 2. *Properties of labeled phage. (A) Effect of increasing fluorochrome labeling (VT680) on phage affinity determined by ELISA (blue region: error range). (B) Effect of increasing labeling on phage fluorescence. Beyond 800 fluorochromes per M13 phage, there is little increase in fluorescence. (C) VT680-labeled phage clone (800 fluorochromes/phage) binds specifically to SPARC-expressing fibroblasts, but not to fibroblasts derived from SPARC$^{-/-}$ mice (scale bar: 10 μm). (D) Effect of successive phage labeling on viability (ability of the phage to infect and amplify in* E. coli*).*

SPARC protein. Regardless of the extent of phage coat protein modification (up to 2400 fluorochromes/phage particle), derivatized phage bound with the same affinity to SPARC protein, as analyzed through ELISA (Figure 2*A*). To maximize the net fluorescence per phage and to enhance signal for *in vivo* imaging, we next measured fluorescence *versus* the extent of fluorochrome labeling. Beyond 800 fluorochromes per phage, fluorescence did not improve significantly presumably due to dye–dye quenching (Figure 2*B*). Importantly, at this extent of modification, labeled phages still retained their biologic targeting ability in that they were able to bind to SPARC (Figure 2*A*). Indeed, in cell-based screens, phages were shown to bind specifically to SPARC-expressing cells but not to fibroblasts isolated from SPARC$^{-/-}$ knockout mice (Figure 2*C*). Taken together, these results demonstrate an optimum labeling of 800 fluorochrome/phage. Therefore, in subsequent experiments, we used phage with 800 fluorochromes attached, corresponding to ~ 25% of coat protein modification. The ability of labeled phage to infect host bacteria and to amplify (viability) was affected in a concentration-dependent fashion (Figure 2*D*). However, at the dose used for *in vivo* experiments, 50% of phages were viable and still permitted regeneration of phage clones when necessary. Similar experiments, as described above, were also conducted with VT680-labeled wild-type and AF750-labeled SPARC and wild-type phages, showing similar results (data not shown).

To determine the time course of biologic uptake and system detection levels of fluorochrome-labeled phage, we next tested labeled phage in a mouse tumor model. LLC cells expressing SPARC [37] were grown in mice until tumors had reached a diameter of 7 to 10 mm. Subsequently, mice were injected intravenously with 10 nmol (fluorochrome concentration) of fluorochrome-labeled phage and serially monitored by FMT [38]. Maximum tumor signal occurred 2 to 4 hours after systemic injection of phage (Figure 3*A*). In dose escalation studies (Figure 3*B*), tumoral signal intensity was highest with the largest amount of phage injected. At this level of phage labeling, the detection threshold by FMT was calculated to be ~ 300 phage/mm^3. Surface reflectance imaging (rapid screening) demonstrated preferential tumoral accumulation of SPARC-targeted phage over wild-type phage (Figure 3*C*). To quantitate variability in tumoral distribution and heterogeneity, we also performed tomographic FMT imaging (Figure 4). Screening experiments showed that SPARC-targeted clones accumulated in all bilaterally implanted LLC tumors (Figure 4*A*), whereas VT680-labeled wild-type phage did not (11,481.92 ± 977 FU in VT680-SPARC phage *versus* 776.01 ± 24 in VT680-WT phage; $P < .0001$; specificity ratio = 14.7; $n = 10$). Serial sections through tumors clearly identified intratumoral phage in a somewhat heterogeneous distribution, which corresponded well with correlative fluorescence microscopy (Figure 5). By FMT measurements, the mean tumoral concentration of SPARC phage was determined to be 23,600 phage/mm^3 or 0.297 pM phage. Although a difference between wild-type and SPARC phage accumulation was noted when they were imaged using surface-weighted fluorescence imaging, a larger difference was seen between the wild-type and SPARC phages when they were imaged with FMT. The ability of FMT to detect fluorescent signal throughout the entire depth of the sample allows for a more precise imaging and opens the door for imaging phage-targeted agents in deep tissues where surface-weighted imaging would not be useful.

We next performed comparative *in vivo* screens of phage clones that had been identified through *in vitro* screens

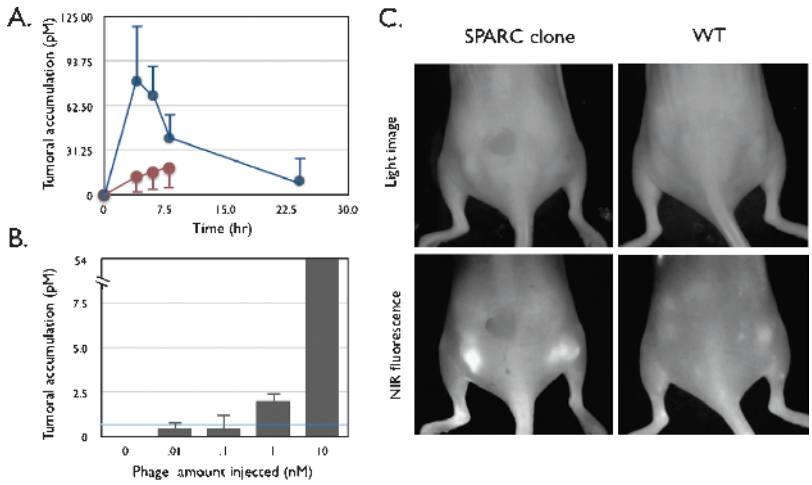

Figure 3. In vivo *behavior of labeled phage. (A) Time course of tumor homing. Mice bearing subcutaneous bilateral LLC-derived tumors were coinjected through the tail vein with VT680-labeled SPARC-targeted phage and AF750-labeled wild-type phage (no insert) and imaged at 0, 2, 4, 6, and 24 hours after injection. Blue line: SPARC-targeted phage clone 23. Brown line: wild-type phage (no insert). (B) Detection threshold. Tumor-bearing mice were injected with increasing log doses of labeled phage and imaged 4 hours after injection. The line indicates detection threshold. (C) Reflectance imaging. Mice bearing subcutaneous bilateral tumors (LLC cells) were injected with either VT680-labeled wild-type phage (right) or VT680-labeled SPARC-targeted phage. Note the brightly fluorescent tumors in the near-infrared fluorescence channel of the SPARC-targeted phage clone [identical white light (WL) settings].*

against SPARC protein, focusing on 5 of 30 ELISA-confirmed clones (Figure 5*A*). There were considerable *in vivo* differences in tumoral homing among lead candidates (Figure 5*B*). Although *in vitro* analysis demonstrated similar specificity constants for the top five lead candidates, *in vivo* testing revealed that phage clone 23 (SPPTGIN) demonstrated excellent *in vivo* targeting ability, whereas clone 12 (NFPQRFL), clone 18 (APTRYNG), clone 21 (HWGMWSY), and clone 26 (GETRAPL) showed much lower *in vivo* homing to tumors (Figure 5*A*). These observations held true among different animals in each group, indicating that homing was not due to individual tumor heterogeneity but rather due to *in vivo* targeting. Furthermore, coinjection of mice with AF750-labeled wild-type phage did not show appreciable targeting (Figure 5*A*), demonstrating the *in vivo* tumor targeting of identified peptide sequences. Additional histologic experiments confirmed the imaging findings (Figure 5*C*).

To determine whether fluorochrome-labeled phage could also be used for microscopic imaging and to extend the technique past one *in vivo* system, we finally performed intravital confocal imaging experiments (Figure 6). Using the TNFα-induced endothelial VCAM-1 upregulation model [10], we performed microvascular imaging in the ear of live mice (Figure 6). Similarly as described above, VCAM-1 internalized phages (bearing the sequence CVHSPNKKC) [10] were labeled with VT680 and injected intravenously 4 hours before imaging. To unequivocally identify microvessels, we coinjected a circulating vascular maker. At the time of imaging, near-infrared fluorescence attributed to phage was highly elevated in the vasculature of the inflamed ear, but was largely absent in the contralateral control ear. There was excellent correlation between local phage homing and signal from the intravascular agent (Figure 6*A*). Immunohistochemistry confirmed the expression of VCAM-1

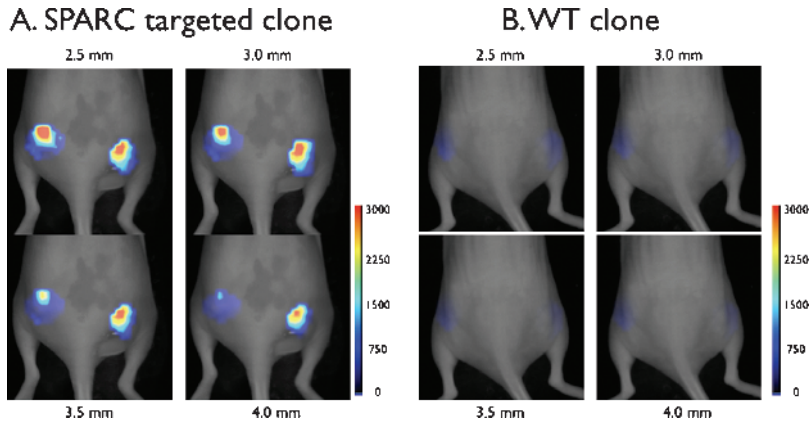

Figure 4. In vivo *imaging of labeled phage. Mice bearing subcutaneous bilateral tumors (LLC cells) were injected with fluorescent phage. (A) Serial coronal tomographic images at different depths of a representative mouse injected with the SPARC-targeted phage clone. Note the distribution of phages throughout the tumors. The scale bar is in nanomolars of fluorescence. (B) Wild-type control phage (identical white light settings as in A).*

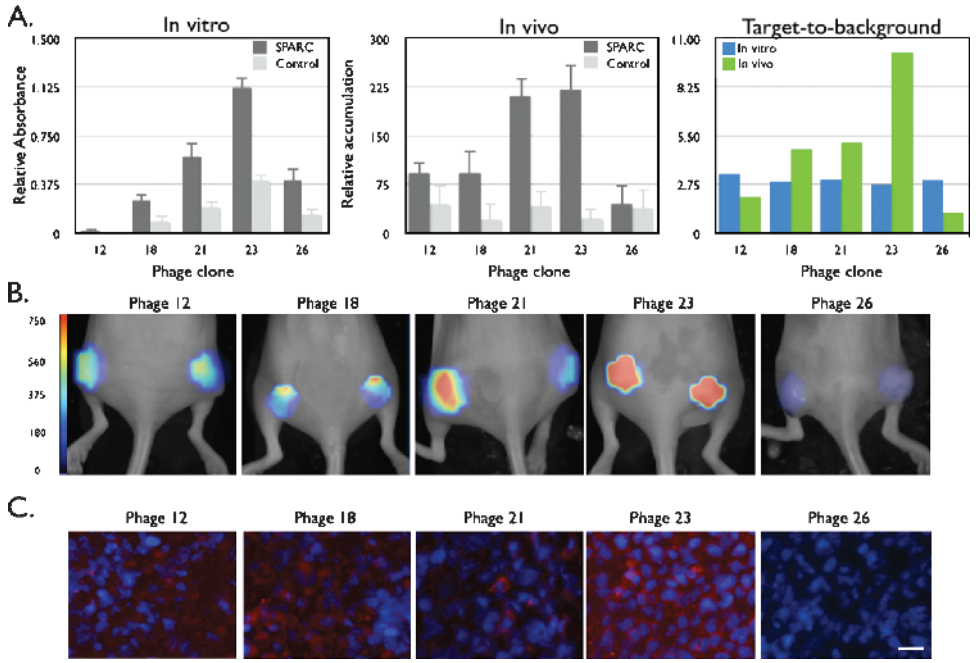

Figure 5. *Screening of SPARC-targeted phage clones. (A) Comparison of the target affinity of different SPARC clones by* in vitro *(left) or* in vivo *(middle and right) imaging (control ELISA: BSA; control FMT: wild-type phage). Note the high target-to-background ratio of clone 23* in vivo*, whereas most clones are similar by* in vitro *screening. (B) FMT imaging of mice bearing bilateral LLC tumors injected with different phage clones. Maximum intensity projections are shown for the five phage constructs investigated. All images have been equally leveled. The scale bar is presented as the concentration of fluorochromes in nanomolars. (C) Comparative immunofluorescence of indicated phage clones' tumoral accumulation (red). Nuclei are counterstained with DAPI (blue). Scale bar = 10 μm.*

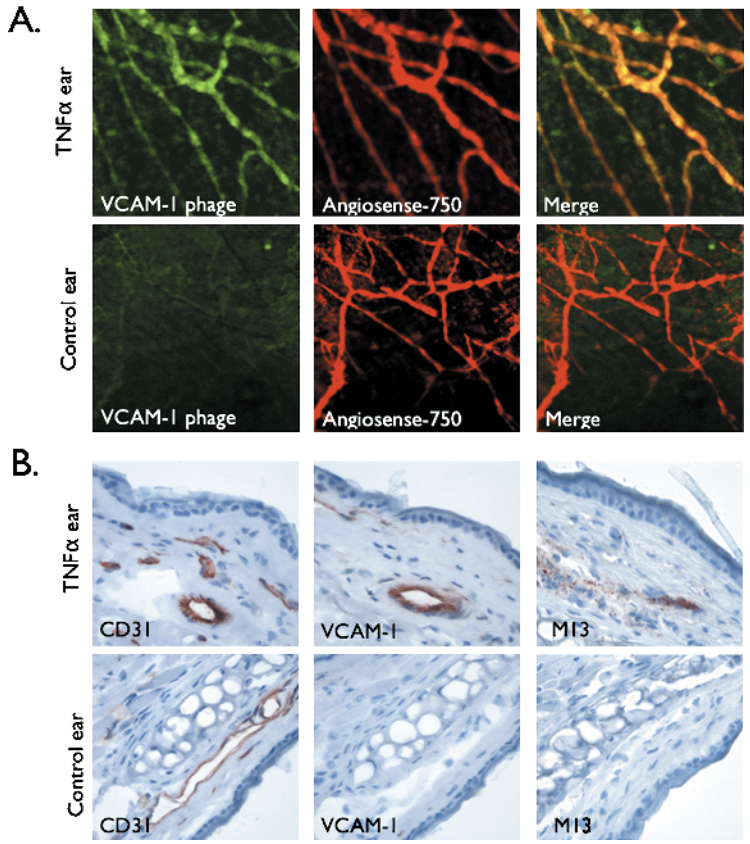

Figure 6. In vivo *microscopic imaging of phage. (A) Microscopic imaging of bilateral ear vessels of a live mouse injected with labeled VCAM-1–targeted phage (CVHSPNKKC, green) and vascular marker (Angiosense-750, red). Shown are confocal projections of Z stacks from mTNFα-treated ear or control ear at 4 hours after phage injection. Images are representative of different animals in each case and five different fields per ear. (B) Correlative histology: adjacent sections of ears taken from* in vivo *intravital experiments were stained for CD31, VCAM-1, or phage protein pVIII (M13).*

in the TNFα-injected ear, but not in the control ear (Figure 6*B*). In addition, phage particles colocalized with VCAM-1–expressing vessels, confirming the retention of phage specificity for VCAM-1 and the use of this technique for *in vivo* imaging (Figure 6*B*).

Discussion

The use of phage display libraries is a powerful method for identifying affinity peptides for biologic applications. For example, phage display has been used to identify vascular zip codes [18], markers of angiogenesis [22], targeted therapeutics [39], or affinity ligands for imaging [10,19]. However, the *in vivo* validation of *in vitro* hits can remain challenging, time-consuming, and costly. Here, we describe methods to label phages with far-red fluorochromes and to test them *in vivo* by optical imaging. This approach is universal, fast, cost-effective, and accurate as multiwavelength imaging can incorporate control phage. The described method enhances *in vivo* phage screening as it allows the direct visualization of injected phage and the identification of cell type–specific clones. In addition, the method is useful for *in vivo* testing whole phage libraries, subsets, or specific clones. Furthermore, we show that near-infrared–labeled phages themselves can serve as an economical and replenishable source of molecularly targeted imaging agents.

Labeling of phage can be accomplished with different available fluorochromes that are well established, yielding highly fluorescent targeted phage particles. M13 filamentous phage (6.5 nm in diameter, ~ 880 nm in length) contains approximately 2700 copies of the major coat protein P8 and 5 copies of three different minor coat proteins (P9, P6, and P3) on the ends. Our results indicate that labeling of coat proteins (800 fluorochromes/phage or ~ 25% of coat proteins) does not interfere with a displayed peptide's targeting ability or a phage's ability to be internalized into mammalian cells (Figure 2*C*). Because we only label 25% of phage coat proteins, the probability of labeling the major coat protein (2700 copies/phage)—as opposed to labeling the peptide (5 copies/phage)—that confers targeting ability is high, therefore allowing the retention of selected biologic activity. Indeed, the six phage clones examined (five SPARC and one VCAM-1) all retained their biologic activity. *In vivo*, we were able to measure the tumor concentration of phage with a threshold of ~ 300 pfu/mm^3. On microscopic resolution, we estimate that the detection threshold is much lower (~ 10 pfu/mm^3) based on confocal laser scanning experiments [34]. The availability of fluorochromes with different spectral properties (Figure 1) allows multicolor imaging (i.e., measurements can be made using a control reference channel) or screening of differently labeled phages simultaneously. These strategies can be exploited to rapidly eliminate clones that would ultimately fail because of unfavorable *in vivo* pharmacokinetics, delivery barriers, or insufficient target-to-background ratios.

We focused on two different model targets in this research, SPARC and VCAM-1, given their importance in human disease [29,31]. SPARC (osteonectin) is a 32-kDa glycoprotein that interacts with the extracellular matrix and exerts an antiadhesive promigratory effect on cells [29]. *In vivo*, SPARC expression is restricted to rapidly remodeling tissues, such as invasive cancers [40]. SPARC has recently been used as a biomarker to identify invasive and/or high-metastatic-potential prostate cancer [29], distinguishing it from more indolent forms. We identified one novel phage clone (23-SPPTGIN) that had high affinity and specificity for SPARC and demonstrated excellent *in vivo* tumoral targeting ability, suggesting that this agent may be useful for the detection and targeting of invasive SPARC-expressing cancers. Conversion of the identified targeted peptide into imaging agents detectable by magnetic resonance imaging and/or positron emission tomography imaging modalities is currently under way. The second example chosen was a phage with high *avidity* (and endothelial cell internalization) for VCAM-1 expression (CVHSPNKKC). We show that fluorescently labeled clones specifically target VCAM-1–expressing blood vessels *in vivo* and could be used for the imaging of VCAM-1 expression in high-mortality diseases such as atherosclerosis.

The developed *in vivo* screening tool could be used to decrease the time between the identification of potential "hits" and the development of *in vivo* molecularly targeted imaging agents. This could potentially eliminate a number of failed "hits" earlier in the investigation, reducing time and cost. Furthermore, we believe that near-infrared tagged phage could play an important role as a molecularly targeted imaging agent. M13 phage particles have the same width and ability to be functionalized as some synthetic nanomaterials currently being used *in vivo* [11,41,42] and have been used here as a platform for the development of imaging agents. Infection with filamentous phages is not lethal as they have been injected intravenously [26]. Furthermore, phages have no intrinsic tropism for mammalian cells and are biodegradable. Phages have also been engineered to serve as delivery vehicles, suggesting that the targeted labeled phage can be used for both imaging and therapy [43].

Acknowledgements

The authors acknowledge E. Aikawa for assistance with immunohistochemistry, F. Reynolds for chemistry assistance, M. Pittet for manuscript review and many helpful discussions, R. Anbazhagan for help with phage cultures, and V. Lok for the performance of histology.

References

[1] Hoffman JA, Giraudo E, Singh M, Zhang L, Inoue M, Porkka K, Hanahan D, and Ruoslahti E (2003). Progressive vascular changes in a transgenic mouse model of squamous cell carcinoma. *Cancer Cell* **4,** 383–391.

[2] Joyce JA, Laakkonen P, Bernasconi M, Bergers G, Ruoslahti E, and Hanahan D (2003). Stage-specific vascular markers revealed by phage display in a mouse model of pancreatic islet tumorigenesis. *Cancer Cell* **4,** 393–403.

[3] Valadon P, Garnett JD, Testa JE, Bauerle M, Oh P, and Schnitzer JE (2006). Screening phage display libraries for organ-specific vascular immunotargeting *in vivo*. *Proc Natl Acad Sci USA* **103,** 407–412.

[4] Zurita AJ, Arap W, and Pasqualini R (2003). Mapping tumor vascular diversity by screening phage display libraries. *J Control Release* **91,** 183–186.
[5] Ladner RC, Sato AK, Gorzelany J, and de Souza M (2004). Phage display–derived peptides as therapeutic alternatives to antibodies. *Drug Discov Today* **9,** 525–529.
[6] Frank R and Hargreaves R (2003). Clinical biomarkers in drug discovery and development. *Nat Rev Drug Discov* **2,** 566–580.
[7] Rudin M and Weissleder R (2003). Molecular imaging in drug discovery and development. *Nat Rev Drug Discov* **2,** 123–131.
[8] Perez JM, Josephson L, O'Loughlin T, Hogemann D, and Weissleder R (2002). Magnetic relaxation switches capable of sensing molecular interactions. *Nat Biotechnol* **20,** 816–820.
[9] Hood L, Heath JR, Phelps ME, and Lin B (2004). Systems biology and new technologies enable predictive and preventative medicine. *Science* **306,** 640–643.
[10] Kelly KA, Allport JR, Tsourkas A, Shinde-Patil VR, Josephson L, and Weissleder R (2005). Detection of vascular adhesion molecule-1 expression using a novel multimodal nanoparticle. *Circ Res* **96,** 327–336.
[11] Akerman ME, Chan WC, Laakkonen P, Bhatia SN, and Ruoslahti E (2002). Nanocrystal targeting *in vivo*. *Proc Natl Acad Sci USA* **99,** 12617–12621.
[12] Zitzmann S, Mier W, Schad A, Kinscherf R, Askoxylakis V, Kramer S, Altmann A, Eisenhut M, and Haberkorn U (2005). A new prostate carcinoma binding peptide (DUP-1) for tumor imaging and therapy. *Clin Cancer Res* **11,** 139–146.
[13] Mikawa M, Wang H, Guo L, Liu R, Marik J, Takada Y, Lam K, and Lau D (2004). Novel peptide ligands for integrin alpha 4 beta 1 overexpressed in cancer cells. *Mol Cancer Ther* **3,** 1329–1334.
[14] Stockwell BR, Haggarty SJ, and Schreiber SL (1999). High-throughput screening of small molecules in miniaturized mammalian cell–based assays involving post-translational modifications. *Chem Biol* **6,** 71–83.
[15] Weissleder R, Kelly K, Sun EY, Shtatland T, and Josephson L (2005). Cell-specific targeting of nanoparticles by multivalent attachment of small molecules. *Nat Biotechnol* **23,** 1418–1423.
[16] Drees BL (1999). Progress and variations in two-hybrid and three-hybrid technologies. *Curr Opin Chem Biol* **3,** 64–70.
[17] Brown CK, Modzelewski RA, Johnson CS, and Wong MK (2000). A novel approach for the identification of unique tumor vasculature binding peptides using an *E. coli* peptide display library. *Ann Surg Oncol* **7,** 743–749.
[18] Rajotte D, Arap W, Hagedorn M, Koivunen E, Pasqualini R, and Ruoslahti E (1998). Molecular heterogeneity of the vascular endothelium revealed by *in vivo* phage display. *J Clin Invest* **102,** 430–437.
[19] Landon LA and Deutscher SL (2003). Combinatorial discovery of tumor targeting peptides using phage display. *J Cell Biochem* **90,** 509–517.
[20] Smith GP and Petrenko VA (1997). Phage display. *Chem Rev* **97,** 391–410.
[21] Willats WG (2002). Phage display: practicalities and prospects. *Plant Mol Biol* **50,** 837–854.
[22] Koivunen E, Gay DA, and Ruoslahti E (1993). Selection of peptides binding to the alpha 5 beta 1 integrin from phage display library. *J Biol Chem* **268,** 20205–20210.
[23] Hong FD and Clayman GL (2000). Isolation of a peptide for targeted drug delivery into human head and neck solid tumors. *Cancer Res* **60,** 6551–6556.
[24] Brown KC (2000). New approaches for cell-specific targeting: identification of cell-selective peptides from combinatorial libraries. *Curr Opin Chem Biol* **4,** 16–21.
[25] Liu C, Bhattacharjee G, Boisvert W, Dilley R, and Edgington T (2003). *In vivo* interrogation of the molecular display of atherosclerotic lesion surfaces. *Am J Pathol* **163,** 1859–1871.
[26] Arap W, Kolonin MG, Trepel M, Lahdenranta J, Cardo-Vila M, Giordano RJ, Mintz PJ, Ardelt PU, Yao VJ, Vidal CI, et al. (2002). Steps toward mapping the human vasculature by phage display. *Nat Med* **8,** 121–127.
[27] Brown EB, Campbell RB, Tsuzuki Y, Xu L, Carmeliet P, Fukumura D, and Jain RK (2001). *In vivo* measurement of gene expression, angiogenesis and physiological function in tumors using multiphoton laser scanning microscopy. *Nat Med* **7,** 864–868.
[28] Massoud TF and Gambhir SS (2003). Molecular imaging in living subjects: seeing fundamental biological processes in a new light. *Genes Dev* **17,** 545–580.
[29] De S, Chen J, Narizhneva NV, Heston W, Brainard J, Sage EH, and Byzova TV (2003). Molecular pathway for cancer metastasis to bone. *J Biol Chem* **278,** 39044–39050.
[30] Koukourakis MI, Giatromanolaki A, Brekken RA, Sivridis E, Gatter KC, Harris AL, and Sage EH (2003). Enhanced expression of SPARC/osteonectin in the tumor-associated stroma of non–small cell lung cancer is correlated with markers of hypoxia/acidity and with poor prognosis of patients. *Cancer Res* **63,** 5376–5380.
[31] Cybulsky MI and Gimbrone MAJ (1991). Endothelial expression of a mononuclear leukocyte adhesion molecule during atherogenesis. *Science* **251,** 788–791.
[32] Funovics M, Montet X, Reynolds F, Weissleder R, and Josephson L (2005). Nanoparticles for the optical imaging of tumor E-selectin. *Neoplasia* **7,** 904–911.
[33] Montet X, Ntziachristos V, Grimm J, and Weissleder R (2005). Tomographic fluorescence mapping of tumor targets. *Cancer Res* **65,** 6330–6336.
[34] Alencar H, Mahmood U, Kawano Y, Hirata T, and Weissleder R (2005). Novel multiwavelength microscopic scanner for mouse imaging. *Neoplasia* **7,** 977–983.
[35] Binstadt BA, Patel PR, Alencar H, Nigrovic PA, Lee DM, Mahmood U, Weissleder R, Mathis D, and Benoist C (2006). Particularities of the vasculature can promote the organ specificity of autoimmune attack. *Nat Immunol* **7,** 284–292.
[36] Weissleder R and Ntziachristos V (2003). Shedding light onto live molecular targets. *Nat Med* **9,** 123–128.
[37] Brekken RA, Puolakkainen P, Graves DC, Workman G, Lubkin SR, and Sage EH (2003). Enhanced growth of tumors in SPARC null mice is associated with changes in the ECM. *J Clin Invest* **111,** 487–495.
[38] Ntziachristos V, Ripoll J, Wang LV, and Weissleder R (2005). Looking and listening to light: the evolution of whole-body photonic imaging. *Nat Biotechnol* **23,** 313–320.
[39] Arap W, Haedicke W, Bernasconi M, Kain R, Rajotte D, Krajewski S, Ellerby HM, Bredesen DE, Pasqualini R, and Ruoslahi E (2002). Targeting the prostate for destruction through a vascular address. *Proc Natl Acad Sci USA* **99,** 1527–1531.
[40] Framson PE and Sage EH (2004). SPARC and tumor growth: where the seed meets the soil? *J Cell Biochem* **92,** 679–690.
[41] Harisinghani MG, Barentsz J, Hahn PF, Deserno WM, Tabatabael S, van de Kaa CH, de la Rosette J, and Weissleder R (2003). Noninvasive detection of clinically occult lymph-node metastases in prostate cancer. *N Engl J Med* **348,** 2491–2499.
[42] Sipkins DA, Cheresh DA, Kazemi MR, Nevin LM, Bednarski MD, and Li KC (1998). Detection of tumor angiogenesis *in vivo* by $alpha_V beta_3$–targeted magnetic resonance imaging. *Nat Med* **4,** 623–626.
[43] Larocca D, Burg MA, Jensen-Pergakes K, Ravey EP, Gonzalez AM, and Baird A (2002). Evolving phage vectors for cell targeted gene delivery. *Curr Pharm Biotechnol* **3,** 45–57.